

Studying the Nonequilibrium Auger Transition Using the Emission Auger Spectroscopy Data

E. R. Burmistrov^a, * and L. P. Avakyants^a

^aMoscow State University, Moscow, Russia

*e-mail: eugeniconovaloff@yandex.ru

Received April 28, 2021; revised June 22, 2021; accepted October 19, 2021

Abstract—The nonequilibrium Auger transition is studied. The transition consists of a probe electron occupying a vacancy in the valence layer. The probe electron absorbs the energy released as a result of the valence electron transition into the *K*-layer followed by emission from the surface. The nonequilibrium Auger spectrum of electrons is obtained for the first time from the surface made of thin (8–10 atomic layers) Ag₂O silver oxide films on a Si₃N₄ substrate for 8–10 keV probing radiation energy. The probability of escape for non-equilibrium Auger electrons is analyzed depending on the atomic number *Z*. The characteristic amplitude peaks are established. The peaks are consistent with the contribution of nonequilibrium Auger electrons to the signal recorded. A mathematical model describing the dynamics of the nonequilibrium Auger process is developed to estimate its probability, relaxation time, and the cross section of capturing a free charge carrier by a neutral vacancy.

Keywords: Auger spectrum, atomic structures, probe, emission, crystal surface

DOI: 10.1134/S2075113322040074

INTRODUCTION

The methods to study structural features on the basis of the energy distribution of particles emitted from the surface are popular to explore physicochemical properties of solid surface atomic layers. The method of emission Auger spectroscopy is used to obtain the data on the energy profile of atomic shells and the strength of the chemical interatomic bond [1, 2]. The method of probing Auger spectroscopy can be applied to study composition and structure of chemical bonds in solutions of complex organic mixtures, in colloidal compounds, and in solid and gaseous mixtures [3, 4].

Sputtering multicomponent and multiphase surfaces by particles of corpuscular probes is of great interest both from the standpoint of obtaining a better picture of the state of the atoms in the surface layer and from the point of view of solving a number of applied problems [5–7]. This topic was in the center of reports delivered at the international conference SIMS-19 [8] addressing the issue of equilibrium Auger recombination as the principal channel for relaxation in atomic structures in the surface layers.

Previously [9], we put forward and theoretically substantiated the assumption that the Auger recombination mechanism can deviate from equilibrium during elastic interaction of particles in surface layers. The essence of the nonequilibrium Auger transition is that the atomic system discards excess energy through

emitting Auger electrons having the energy higher than that of the incident probing particles [9]. This mechanism is similar to the anomalous Compton effect, as well as to the Raman scattering (Raman effect) with satellite frequencies both higher and lower than that of exciting electromagnetic radiation [10, 11].

We determined the parameters of the probing radiation and those of the test sample resulting in a non-equilibrium dynamic effect. The energy spectrum of nonequilibrium Auger electrons emitted from the test surface was obtained for the first time. Inelastic interaction of high-energy particles of probing radiation with electrons of the *K*-layer results in a vacancy which is filled with a valence electron of the studied atomic structure. It was suggested in [9] that the nonequilibrium Auger transition consists in that the vacancy formed in the valence layer is filled with a probe electron obtaining the energy released as a result of the valence electron transiting to the *K*-layer and emitting from the surface. The calculations presented in [9] indicate that the relaxation of the atomic structure accompanied by emission of a nonequilibrium Auger electron had a relaxation time of $\sim 10^{-14}$ s.

It is difficult to identify the local spectral maxima corresponding to nonequilibrium Auger electrons as there is a strong background of the secondary and inelastically scattered Auger electrons present in the spectrum [12–14]. Therefore, the spectrum should undergo mathematical processing to identify the signal

corresponding to nonequilibrium Auger electrons. This processing involves selecting and studying in detail the spectral region corresponding to all electrons that are generated by the Auger process. The studies allowed establishing characteristic amplitude peaks corresponding to the contribution of nonequilibrium Auger electrons to the signal detected. Being based on the mathematical model developed in [9] to describe the dynamics of the nonequilibrium Auger process, its probability, relaxation time, and the capture cross section of a free charge carrier by a neutral vacancy were calculated. The Auger spectra obtained were processed by increasing the scale of the selected energy domain, followed by taking the second derivative with subsequent approximation of the experimentally obtained dependence. This processing was necessary to suppress the background of the secondary electrons and reveal the features typical of nonequilibrium Auger electrons.

SAMPLES

The probability of escape of a nonequilibrium Auger electron depends on the atomic number Z of elements composing the surface. The probability of a radiation transition increases with growing atomic number in proportion to Z^4 , reaching 90% for chemical elements with $Z > 75$. When the surface consisting of atoms having a small mass number is sputtered using an electron beam, the dominant mechanism of relaxation deals with relaxation of the valence atomic layers following the principle of radiation-free nonequilibrium Auger transition.

With consideration of these features, the samples were grown using the atomic layer deposition from the gas phase of the sprayed substance onto the substrate having the selected adhesive properties. The samples to be studied were obtained using the ALD P-1000 Picosun installation through a successive deposition of monatomic layers, which enabled continuous monitoring of the properties of the deposited coating. The samples comprised thin films obtained through depositing silver oxide Ag_2O on a Si_3N_4 substrate 2.5 μm thick. Further annealing at a temperature of 170°C was carried out in order to convert Ag_2O into the cubic η -phase and eliminate contaminants. The initial parameters of deposited coatings, as well as properties of the probing radiation, are given in Table 1.

The following notation is used in Table 1: N is the number of Ag_2O atomic layers deposited on the insulating GaN substrate, S is the area of the deposited coating, ρ is the packing density in the Ag_2O crystal structure, E is the energy of the primary probing radiation of incident electrons, and D is the diameter of the primary electron beam.

It was found in [9] that the nonequilibrium Auger transition was most likely observed in elements with $Z < 60$. These include Br, Mo, Ag, and In. A small

Table 1. Initial parameters of probing radiation and Ag_2O samples

Sample series	N	S, mm^2	$\rho, \text{g/cm}^3$	E, keV	$D, \mu\text{m}$
1	12	110×60	17.22	8	1.2
2	18	100×55	18.01	11	
3	22	124×58	17.68	14	

thickness of the sample (of the order of 8–10 atomic layers) depends on the exponential relationship between the depth of the atom and the number of non-equilibrium Auger electrons that can penetrate the layer having thickness d and enter the vacuum without scattering on phonons and on electron shells of other atoms:

$$N = N_0 \exp(-d/\lambda), \quad (1)$$

where λ is the free path, which can be determined according to the empirical formula [9]

$$\lambda = 520E^{-2} + 0.32a\sqrt{E}, \quad (2)$$

where a is the thickness of a single Ag_2O monolayer.

Under experimental conditions, the energy of the incident electrons lies within the range of binding energies between K -layer electrons and the nucleus in Ag_2O . This is due to the fact that capturing a free electron by a neutral vacancy and subsequent nonequilibrium Auger transition occur on the inner shells of atoms [9]. The beam was 1.2 μm wide, which was sufficient to provide the local impact of the probing beam on the sample surface.

An assumption that the electron density in the surface layer is high and the transition time between $4p^1$ and $1s^1$ states is sufficiently short compared to the time of filling the $4p^2$ state with a probe electron is important to trigger nonequilibrium Auger transition. Indeed, when a probe particle knocks out an electron from the K -layer, a vacancy is formed, which can be occupied by a probe particle. It is necessary that the $4p^1$ electron have time to fill it, implying that the density of the electron environment should be sufficiently high at the location of the atom.

EXPERIMENTAL

Auger spectra were registered using a PHI-670 Xi scanning Auger electron spectrometer, the schematic diagram of which is depicted in Fig. 1.

The samples were fixed in holder 2 and exposed to probing radiation emitted by electron gun 3. The flow of electrons sputtered from the surface studied is rather small; therefore, guided by the focusing system 1, the flow was amplified using electron multiplier 7. The electrical signal of the secondary and Auger electrons was generated by synchronous detector 8. Further pro-

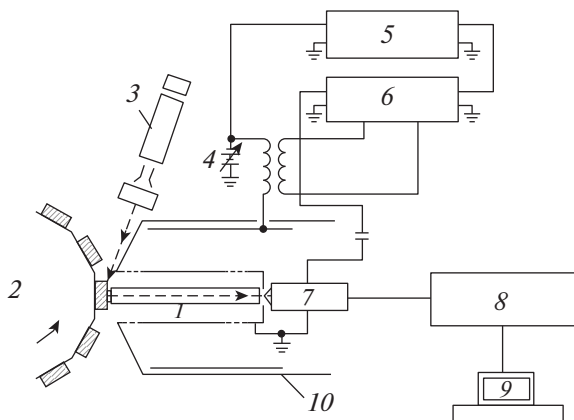


Fig. 1. Schematic diagram of a scanning Auger spectrometer: (1) focusing system; (2) pivoting sample holder; (3) electron gun; (4) voltage source; (5) oscilloscope; (6) synchronous detector; (7) electron multiplier; (8) detector; (9) computer (visualizing the Auger spectrum); (10) magnetic shield.

filling and processing of the Auger spectrum recorded in the experiment was carried out using computer 9. Thus, the sputtering of Ag_2O plates using the primary electron beam and subsequent recording the Auger spectrum were carried out under high vacuum conditions of $\sim 10^{-5}$ Pa at room temperature. The energy of the particles registered at the output lies in the range of 20–1500 eV.

EXPERIMENTAL RESULTS AND DISCUSSION

The Auger spectra obtained are shown in Fig. 2 together with experimental samples. The spectrum shows an upcoming segment of the amplitude peak corresponding to the secondary scattered electrons, as well as an energy region characterizing the contribution of Auger electrons to the overall relaxation channel. This area is most interesting for further studies into nonequilibrium Auger process.

The position of the maxima corresponding to non-equilibrium Auger transitions can be determined with an accuracy of ± 5 eV, while an increase in the selectivity of the Auger analysis from the surface of a film or from a solid results in inevitable narrowing of the intensity and the bandwidth of the energy analyzer. Consequently, a significant part of information about the state of the surface under study is lost, specifically, owing to suppression of the signal of interest by the background of the secondary and inelastically scattered Auger electrons. In order to identify local peaks, the Auger spectrum was amplified by a factor of 10, followed by taking the derivative $f(E) = dN(E)/dE$, as shown in Fig. 3a. Also, Fig. 3b shows the result of taking the second derivative of the initial Auger spectrum. This allowed finding the spectral lines corresponding to the frequencies of the fundamental transitions of

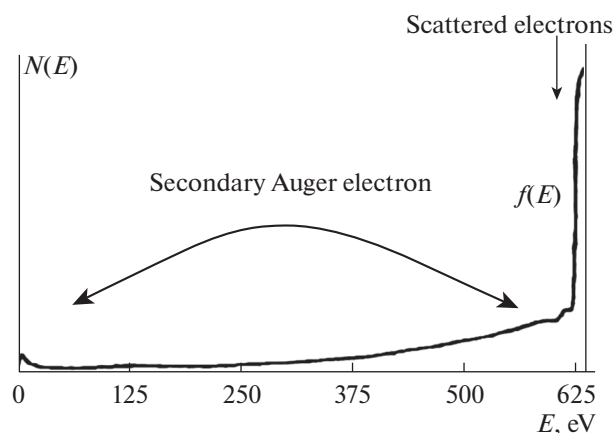


Fig. 2. Auger spectrum obtained for Ag_2O plates grown by atomic layer deposition on a Si_3N_4 substrate with the probing radiation energy equal to 8 keV. Plotted along the y axis is the particle count intensity $N(E)$ in the secondary flow as a function of energy; $f(E)$ is the experimental curve.

the valence electrons in the $4d$ and $5p$ shells in the Ag atom. The presence of a spectral line corresponding to the last transition indicates that silver atoms are present in the excited state.

The experimental data confirmed that the spectral width of the local maximum shown in Fig. 3b is controlled by presence of nonequilibrium Auger electrons in the secondary flow. Indeed, nonequilibrium Auger electrons emitted from the surface cannot amplify the signal or produce a discrete set of lines since they have low intensity in the secondary flow. However, as can be seen from Fig. 3b, they provide the main contribution to the increasing section of the derivative and broaden the local maximum. The line width of the spectrum is equal to 5 eV. This is the lower limit to detect nonequilibrium Auger spectra, starting from which the intensity of their emission from the surface of the sample grows with increasing energy of the incident electrons. This results in broadening of the local maximum (Fig. 4). As can be seen from comparing the spectra shown in Figs. 3 and 4, the local maximum is broadened to 10 eV with an increase in the probing radiation energy from 8 to 14 keV. This explains the growing share of nonequilibrium Auger electrons contributing to the general atomic structure relaxation channel in the surface layer. As the energy of the incident particles of the probe increases, the fraction of nonequilibrium Auger electrons increases in the secondary flow, which leads to broadening of the spectral line in the higher energy domain. This experimental fact confirms the assumption made in [9] about broadening of the spectral line.

The amplitude peak observed in Figs 3 and 4 is an envelope of discrete spectral lines, which, because of the low intensity, are not observed on the graph. In this case, the half-width of the local maximum, which

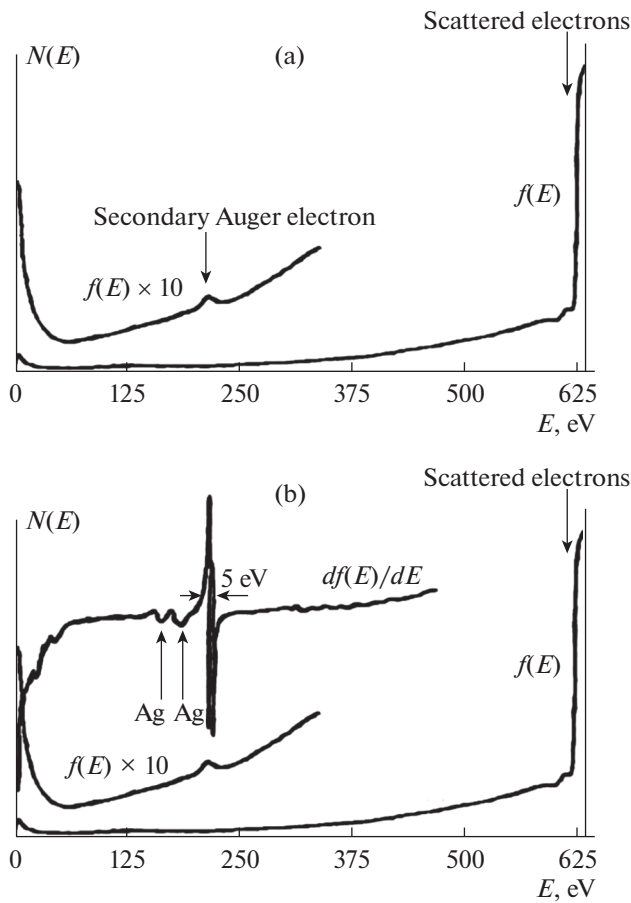


Fig. 3. Processing the Auger spectrum obtained for Ag_2O plates: (a) segment of the first derivative of the Auger spectrum amplified by a factor of 10 having the local maximum corresponding to the secondary Auger electrons. The spectrum was obtained at an energy of probing radiation of 8 keV. (b) The second derivative of the Auger spectrum and the fundamental transitions of Ag atoms revealed by the second derivative.

lies in the region of high energies, is the envelope of discrete lines corresponding to nonequilibrium Auger electrons in the secondary flow. It was established that the spectral width of the peak recorded for the second derivative of the experimental curve depends on the presence of nonequilibrium Auger electrons in the secondary flow, which, in turn, confirms the assumption made in [9] about existence of a nonequilibrium Auger transition.

The probability of a nonequilibrium Auger transition was calculated using the first order of perturbation theory describing electron-electron interactions [9]

$$\begin{aligned} W_A &= \frac{2\pi}{\hbar} |M_{fi}|^2 \delta(E_f - E_i) \\ &= \frac{2\pi}{\hbar} \rho(\vec{k}) \left| \iint \phi_f(\vec{r}_1) \psi_f(\vec{r}_2) \right. \\ &\quad \times U(\vec{r}_1, \vec{r}_2) \phi_i(\vec{r}_1) \psi_i(\vec{r}_2) dV_1 dV_2 \left. \right|^2, \end{aligned} \quad (3)$$

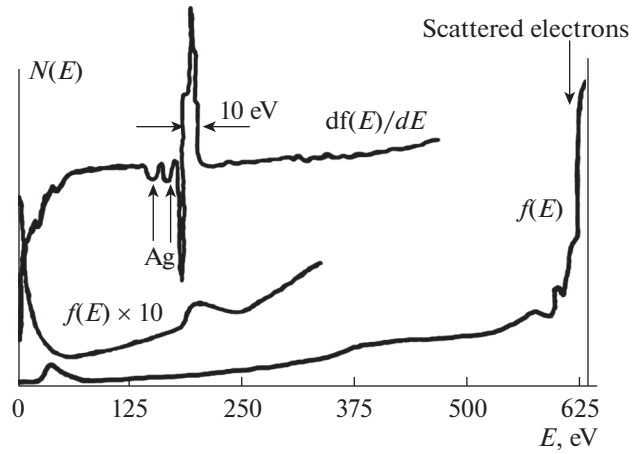


Fig. 4. Amplified (10 \times) initial part of the first and the second derivatives of the Auger spectrum featuring the local maximum corresponding to the secondary Auger electrons. The spectrum was obtained for a probing radiation energy of 14 keV.

where M_{fi} is the matrix element of the Coulomb interaction, $\rho(\vec{k}) = mV|\vec{k}| \cdot d\Theta/8\pi^3\hbar^2$ is the normalized density of states reduced to a box having volume V , $d\Theta = \sin\Theta d\Theta d\varphi$ is the element of solid angle, $|\vec{k}|$ is the modulus of the wave vector, $\hbar = 1.055 \times 10^{-34}$ J s, $e = 1.6 \times 10^{-19}$ K, and $U(\vec{r}_1, \vec{r}_2) = e^2/(\vec{r}_1 - \vec{r}_2)$ is the interaction potential.

Taking into account the small radial component of the wave function in the s -state compared to the wave function in p -state, we can roughly approximate the interaction potential as follows:

$$\begin{aligned} e^2/(\vec{r}_1 - \vec{r}_2) &\approx (e^2/\vec{r}_2)(1 + (\vec{r}_1/\vec{r}_2)\cos\theta_{12}) \\ &= e^2(1/\vec{r}_2 + (\vec{r}_1/\vec{r}_2)^2)(C_1C_2 + S_1S_2)), \end{aligned} \quad (4)$$

where $C_1 = \cos\theta_1$, $C_2 = \cos\theta_2$, $S_1 = \sin\theta_1$, and $S_2 = \sin\theta_2$; $Y_{10}(\theta_2, \varphi_2) = \frac{i}{2} \sqrt{\frac{3}{4\pi}} C_2 = A$.

The final expression used to calculate the probability of a nonequilibrium Auger transition has the form [9]

$$\begin{aligned} W_A &= R' \left\{ \iint \iint A^2 e^{(-1/a(2\vec{r}_1 + \vec{r}_2))} \right. \\ &\quad \times (1/\vec{r}_2 + (\vec{r}_1/\vec{r}_2)^2)(C_1C_2 + S_1S_2))^2 \\ &\quad \times \vec{r}_2^2 \vec{r}_1^2 \vec{r}_2^2 S_1 S_2 d\vec{r}_1 d\vec{r}_2 d\theta_1 d\theta_2 \Big\} \\ &= R' \left[\iint \iint A^2 e^{(-1/a(2\vec{r}_1 + \vec{r}_2))} \right. \\ &\quad \times \vec{r}_1^2 \vec{r}_1^2 S_1 S_2 d\vec{r}_1 d\vec{r}_2 d\theta_1 d\theta_2 \\ &\quad + 2 \iint \iint A^2 e^{(-1/a(2\vec{r}_1 + \vec{r}_2))} \vec{r}_1(C_1C_2 + S_1S_2) \\ &\quad \times S_1 S_2 d\vec{r}_1 d\vec{r}_2 d\theta_1 d\theta_2 + \iint \iint A^2 r_1^4 e^{(-1/a(2\vec{r}_1 + \vec{r}_2))} \\ &\quad \left. \left. + (C_1C_2 + S_1S_2)^2 S_1 S_2 d\vec{r}_1 d\vec{r}_2 d\theta_1 d\theta_2 \right] \right]. \end{aligned} \quad (5)$$

Table 2. Theoretical values of nonequilibrium Auger transitions

Sample series	Element	W_A , 10^{13} s^{-1} of the nonequilibrium Auger transition	τ , 10^{-14} s	Γ , eV
35	Br	0.78	2.15	5.2
11	Na	0.50	1.98	5.2
12	Mg	0.54	1.82	5.7
13	Al	0.56	1.75	6.2
14	Ag	0.81	1.63	5.0

The results of calculations based on formula (5) are listed in Table 2.

The following designations are accepted in Table 2: Γ is the width of the local maximum observed in the second derivative of the spectrum; W_A and τ are the probability and time of a nonequilibrium Auger transition in an excited atomic structure.

As shown in Table 2, an increase in the atomic number entails spectral broadening with growing probability of a nonequilibrium Auger transition. It should be noted that nonequilibrium Auger electrons released from deeper layers lose energy because of inelastic collisions and do not contribute to the Auger lines, but they significantly broaden them and contribute to the increasing part of the derivative.

These studies also addressed the issue of calculating the cross section of capture of free electrons in a deep trap [15]. The theory of impact ionization within the framework of secondary ion-electron emission was sufficiently developed to estimate the cross section of capture of a free carrier by neutral traps. In particular, the capture cross section amounts to $\sigma_p \sim 10^{-18} \text{ cm}^2$ for high concentrations of free carriers ($n > 10^{18} \text{ cm}^{-3}$) [9]. The results of calculating the cross section of capture of a free carrier by deep traps during nonequilibrium Auger transition are given in Table 3. The calculations were made for three different vacancy depths in the surface layer.

There is the notation taken in Table 3 implying that $\beta = m/m_0$ is the ratio of the effective and true masses of the charge carrier and E_i is the depth of the vacancy. The data listed in Table 3 indicate that the capture cross section decreases with increasing depth of the neutral trap. This dependence is explained by elastic

scattering free carriers at the sites of the crystal lattice and at the electron shells of atoms. Therefore, the effect of the nonequilibrium Auger transition is best observed when the vacancy is localized at a depth of 0.2 to 0.3 eV, as well as when the ratio of the effective to true carrier mass is low.

CONCLUSIONS

It was established that one of the possible channels for relaxing atomic or cluster structures in the surface layers can involve emission of nonequilibrium Auger electrons. It was shown that the process studied competed with the normal Auger recombination with growing number of the chemical element and increasing atomic radius in the surface layer.

The Auger spectrum was obtained experimentally, featuring spectral inhomogeneities corresponding to nonequilibrium Auger electrons present in the secondary flow. A good agreement between the experimental and theoretical data confirmed the assumption made earlier [9] about potential nonequilibrium Auger transition accompanying energy relaxation of atomic structures in surface layers.

A method was developed to make samples and determine their parameters and conditions to observe nonequilibrium Auger transition during excitation of atomic structures using probe electrons. On the basis of the obtained experimental data, it was shown that the relaxation of the atomic structure accompanied by emission of a nonequilibrium Auger electron had a relaxation time of $\sim 10^{-14} \text{ s}$. The probability of a non-equilibrium Auger transition amounted to 10^{13} s^{-1} , and the cross section of capture of a free carrier by a neutral vacancy was $2.1 \times 10^{-18} \text{ cm}^2$.

It is important to note that the presence of non-equilibrium Auger electrons in the secondary flow can be used to estimate the strength of the chemical bond between atoms and assess the electronic structure of atomic shells. In this case, the local elemental analysis can be carried out at the nanometer scale through narrowing of the diameter of the electron beam in electron guns. Thus, an experimental substantiation was obtained for the assumption on potential excitation of a nonequilibrium Auger transition by corpuscular probes. The authors assume that effect of a nonequilibrium Auger transition can be observed both using Auger electron spectroscopy and through excitation of

Table 3. Cross section of capture of free carriers by neutral traps localized in surface layer

Element	E_i^1 , eV	β	σ_p , 10^{-18} cm^2	E_i^2 , eV	β	σ_p , 10^{-18} cm^2	E_i^3 , eV	β	σ_p , 10^{-18} cm^2
Na	0.18	0.2	2.1	0.3	0.2	1.3	0.6	0.2	0.9
Br	0.25	0.6	1.8	0.5	0.6	0.8	0.8	0.6	0.5
Ag	0.3	0.4	1.3	0.7	0.4	0.2	1.1	0.4	0.11

atoms of solids by ions having medium or high energies and probing photons.

REFERENCES

1. Zel'tser, I.A., Kukushkin, S.A., and Moos, E.N., New possibilities in nanoscale surface structure diagnostics using X-ray standing waves under conditions of continuous resonant X-ray Raman scattering, *Tech. Phys. Lett.*, 2008, vol. 34, pp. 568–570.
<https://doi.org/10.1134/S1063785008070092>
2. Abgaryan, V.K., Gidashev, V.Yu., Nadiradze, A.B., et al., Ion–electron recombination and heat fluxes in high-frequency ion thrusters, *Tech. Phys. Lett.*, 2019, vol. 45, pp. 123–125.
<https://doi.org/10.1134/S1063785019020226>
3. Zhigalin, A.S., Roussikh, A.G., Baksht, R.B., et al., Suppression of Rayleigh–Taylor instabilities in Z-pinchers, *Tech. Phys. Lett.*, 2015, vol. 41, pp. 554–556.
<https://doi.org/10.1134/S1063785015060152>
4. Repsilber, T., Borghesi, M., Gauthier, J.-C., et al., Quantitative analysis of proton imaging measurements of laser-induced plasmas, *Appl. Phys. B*, 2005, vol. 80, no. 7, pp. 905–913.
<https://doi.org/10.1007/s00340-005-1800-y>
5. Faenov, A.Ya., Skobelev, I.Yu., Pikuz, T.A., et al., Diagnostics of the early stage of the heating of clusters by a femtosecond laser pulse from the spectra of hollow ions, *JETP Lett.*, 2011, vol. 94, art. ID 171.
<https://doi.org/10.1134/S0021364011150033>
6. Landau, L.D. and Lifshitz, E.M., *Course of Theoretical Physics*, vol. 3: *Quantum Mechanics*, Oxford: Pergamon, 1986.
7. Windhorn, L., Witte, T., Yeston, J.S., et al., Molecular dissociation by mid-IR femtosecond pulses, *Chem. Phys. Lett.*, 2002, vol. 37, no. 14, pp. 85–90.
8. Au, M.K., Hackett, P.A., Humphries, M., and John, P., Dynamics of photoprocesses induced by femtosecond infrared radiation in free molecules and clusters of iron pent carbonyl, *Appl. Phys. B*, 2010, vol. 33, no. 43, pp. 56–65.
9. Burmistrov, E.R. and Avakyants, L.P., Possibility of excitation of nonequilibrium Auger transitions by corpuscular probes, *Nanostrukt. Mat. Fiz. Model.*, 2020, vol. 21, no. 1, pp. 37–50.
https://nano-journal.ru/21_1_Burmistrov
10. Makarov, A.A., Malinovsky, A.L., and Ryabov, E.A., Intramolecular vibrational redistribution: From high-resolution spectra to real-time dynamics, *Phys.-Usp.*, 2012, vol. 55, no. 10, pp. 119–127.
11. Gaïdukov, M.M., Gagarin, A.G., Kozyrev, A.B., et al., Microwave losses in metal–ferroelectric–metal thin-film capacitors, *Tech. Phys. Lett.*, 2008, vol. 34, pp. 565–567.
<https://doi.org/10.1134/S1063785008070080>
12. Tagantsev, A.K., Sherman, V.O., and Astafiev, K.F., Ferroelectric materials for microwave tunable applications, *J. Electroceram.*, 2003, vol. 11, no. 1, pp. 5–66.
13. Landsberg, G.S. and Mandelstam, L.I., *J. Russ. Phys. Chem.*, 1928, vol. 345, no. 60, pp. 55–61.
14. Acikel, B., Taylor, T.R., Hansen, P.J., et al., High-resolution transmission electron microscopy of heteroepitaxial barium strontium titanate films grown on MgO substrates, *IEEE Microwave Wireless Compon. Lett.*, 2002, vol. 12, no. 7, pp. 237–239.
15. Mukhortov, Vas.M., Masychev, S.I., Golovko, Yu.I., Chub, A.V., and Mukhortov, V.M., Application of nanodimensional barium-strontium titanate films in tunable microwave devices, *Tech. Phys.*, 2006, vol. 51, no. 10, pp. 1359–1361.
<https://doi.org/10.1134/S1063784206100173>

Translated by V. Vetrov

SPELL: RUBRIC????